

The Influence of Dielectric Thickness on the Power Bandwidth of Planar Transformers

Hyma H. Vallabhapurapu* and Ivan W. Hofsjager

Abstract—This paper considers an ideal planar transformer wherein only the electromagnetic parasitics (stray capacitive and leakage inductance) arising out of the transformer geometry are taken into account, assuming lossless conditions. A suitable electrically equivalent circuit model for the planar transformer is used to analyze its frequency and power transfer characteristics; this model was validated by a three dimensional electromagnetic simulation of the planar transformer structure in FEKO electromagnetic simulation software. The effect of dielectric thickness on the bandwidth of the transformer has been analyzed based on the premise that the inherent stray capacitance and leakage inductance elements would affect the power transfer characteristics of the transformer. It has been found that the dielectric thickness of a planar transformer can be optimized so as to maximize the frequency bandwidth. It is also shown that the bandwidth is found to be sensitive to the thickness of the dielectric beyond the optimum thickness threshold t_{opt} . Convenient closed form analytic expressions for the optimum dielectric thickness and the resultant maximum bandwidth are derived and presented. It is argued that these results can be readily used to benefit the design of air-core PCB/Planar transformers.

1. INTRODUCTION

Planar transformers are a subset of planar magnetics technology, used widely as components in power electronics topologies. One of the first publications on this technology appeared in the year 1986 and was the work of Alexander Estrov [1], which was later patented in 1991 [2]. These transformers are constructed by sandwiching layers of conductors, dielectrics and magnetic materials together [3]. The advantages of planar transformers are that the planar nature of the windings allow for more complex and efficient winding configurations, and also allows for excellent repeatability in manufacturing due to well defined geometry [4–6]. This characteristic allows parasitics to be intelligently controlled such that they have the least effect on the performance of the transformer. Furthermore, planar nature lends to low profile and better heat dissipation qualities [7–10].

Planar transformers often replace traditional transformers for operation frequencies higher than 100 kHz [11] and for power levels in the range of several kVA [12]. Many authors [5, 9, 13–15] cite these characteristics as main reasons to use planar transformers in switched-mode power supplies; the same has allowed authors to develop planar transformers for applications in aerospace [16] and consumer electronics [15, 17, 18].

The need for compact and power-dense planar transformers poses a problem as it is not known how compact these transformers can be constructed.

Several articles [8, 19, 20] state that the bulk of research is focused on the modeling and optimizing of losses and leakage inductance, with little consideration for parasitic capacitance. This practice reflects in the design of planar transformers up to recent times as they have not seriously considered the crucial

Received 18 November 2017, Accepted 7 December 2017, Scheduled 16 January 2018

* Corresponding author: H. H. Vallabhapurapu (hyma.vallabhapurapu@students.wits.ac.za).

The authors are with the School of Electrical and Information Engineering, University of the Witwatersrand, Johannesburg, South Africa.

balance of parasitic capacitance and leakage inductance in the design stages. For example, a custom transformer core was designed [21] in order to achieve a record-worthy power density. In this case, there does not appear to be any motivation to optimally accommodate the electric (stray capacitor) and magnetic (leakage inductor) parasitics. In light of this, the question lingers as to whether a higher power-density could be achieved had the parasitics been optimized. Furthermore, it is also not evident what the immediate trade-off is between the high power-density and the bandwidth of the transformer.

Trade-off between leakage inductance, losses and stray capacitance has been investigated to some extent in [8], and in [4] the authors define a ‘figure-of-trouble’ product LC as being the product of leakage inductance and parasitic capacitance, since both quantities are dependent on the dielectric thickness of the windings in an opposing manner. In both papers, the trade-off has not been thoroughly investigated within the context of bandwidth, leaving room for further research in this direction.

The general view is that both stray capacitance and leakage inductance have an impact on the ‘cutoff frequency’ and ‘bandwidth’ of the transformer respectively [4, 21–23]. However, the bandwidth is yet to be described as functions of these intrinsic electromagnetic parasitic elements. The bandwidth of a planar transformer should be an important design consideration as signals and power waveforms need to pass through the structure undistorted, especially when excited by square-wave sources [24] due to the harmonics.

Currently, the dielectric thickness appears to be chosen based on what is readily available, as long as it does not undergo dielectric breakdown. Examples of standard thicknesses for dielectrics are 0.4 mm, 0.8 mm and 1.6 mm [23]. However, the dielectric thickness is known to have a direct impact on the electromagnetic parasitics (stray capacitance and leakage inductance) within the transformer, which is in turn thought to impact on the transformer’s bandwidth. It is therefore necessary to choose the dielectric thickness in a optimum manner if bandwidth is important to the application. This paper is meant to provide a direction in this regard by finding the optimum dielectric thickness so as to provide the best possible bandwidth for a given application.

It is reasoned that once the optimum dielectric thickness is found, it will lead to the optimum values of stray capacitance and leakage inductance. The added benefit could potentially be a marginal increase in power-density due to the choice of optimum dielectric thickness. Much research has been done to optimize the performance of the planar transformer by merely looking at losses and non-linear frequency dependent material characteristics. This indicates that the optimization of the discussed electromagnetic parasitics is often ignored. Based on this observation, this paper will approach the problem from a different direction, wherein the transformer performance is evaluated solely based on electromagnetic interactions and not losses due to imperfect materials.

2. THE PLANAR TRANSFORMER MODEL

There are two levels of modeling in this paper — the model of the parasitics and the model of the electrical equivalent circuit; both of these are developed based on analysis of the electric and magnetic field distributions within the transformer structure.

Due to the assumptions and constraints that follow, the model and the resulting contribution are best validated through full three-dimensional electromagnetic simulations of the planar transformer structure, where such reasonable conditions can be imposed or controlled. ‘FEKO’ electromagnetic simulation software [25] is used, configured to use the ‘Surface Equivalent Principle’ and automatic mesh density selection.

The following constraints and assumptions are made:

- (i) Although planar transformers come in various shapes, a rectangular form is assumed for this work. The results should hold true for all shapes in general, as long as the electrical model remains the same.
- (ii) The analysis is restricted to non-interleaved planar transformers. All layers of the windings are assumed to have an equal number of turns. All dielectric layers are assumed to be of equal thickness. The dielectric thickness is considered to be generally much larger than the conductor thickness.
- (iii) All losses are ignored, as they have been examined in great detail in literature. Inclusion of these effects would obscure the interactions between the leakage inductance and the stray capacitance,

and would defeat the purpose of the analysis as the theoretical bandwidth limit is to be found. Materials are considered to be ideal, implying that there are no frequency dependent dielectric or magnetic effects. Dielectric breakdown is not explicitly considered.

- (iv) Stray capacitance coupling to the environment is ignored as the determination of these capacitances is complicated due to the unpredictable nature of the environment in practice. As a consequence, common-mode currents are ignored. This implies that the potentials on the secondary side of the transformer do not rise to arbitrary values.

These constraints and assumptions ensure that any results derived from the model are based only on the electromagnetic parasitic elements of the model, that arise intrinsically due to the geometry of the transformer.

The dimensions of the dielectric layer and the magnetic core mentioned throughout the paper are illustrated in Fig. 1 and Fig. 2 respectively. A list of important symbols used throughout the paper is given in Table 1.

Table 1. List of symbols.

SYMBOL	DESCRIPTION
b_w	Core window width
l_c	Core leg length
l_w	Core leg window
l_m	Mean magnetic flux path length
D_l	Dielectric layer side length
D_w	Dielectric layer side width
l	Turn length of the conductor track per layer it is equal to l_t when $n = 1$
l_t	Mean turn length of the dielectric layer
w	Width of the conductor track it is equal to b_w when $n = 1$
t	Thickness of dielectric layer
n	Turns on each dielectric layer
N_L	Number of layers of a winding
$N_{P/S}$	Number of primary/secondary layers
a_r	Transformer turns ratio
E	Electric field strength
H	Magnetic field strength

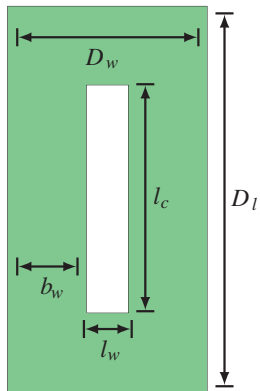


Figure 1. Geometry of the dielectric layer.

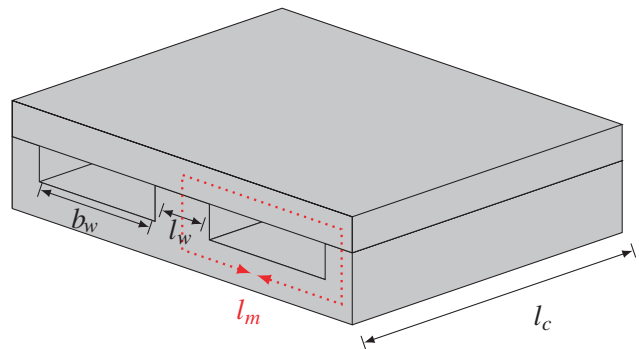


Figure 2. 3D view of the planar core.

2.1. Parasitic Capacitance

The parasitic capacitances arise due to the electric field energy stored inside the dielectric layers of each primary and secondary winding (self capacitance), and due to the energy stored between the primary and secondary winding (coupling capacitance).

The voltage distribution within a winding is analyzed to derive the self capacitance expression. A 4-layer winding is simulated in FEKO, and the simulated voltage distribution is shown in Fig. 3. The integral of the electric field within the winding volume is given as Eq. (1a) with an applied voltage V_a . Using the expression for energy stored in a capacitor, the self capacitance C_x is given as Eq. (1b).

$$\int E^2 dVol = t l w (N_L - 1) \left(\frac{V_a}{t N_L} \right)^2 \quad (1a)$$

$$C_x = \epsilon_0 \epsilon_r \frac{l w}{t} \left(\frac{N_L - 1}{N_L^2} \right) \quad (1b)$$

The gradients of the voltage distribution within the primary and secondary windings are found to be the same due to Faraday's law. The coupling capacitance is thus found to be a simple parallel plate capacitance as given as Eq. (2).

$$C_k = \epsilon_r \epsilon_0 \frac{l w}{t} \quad (2)$$

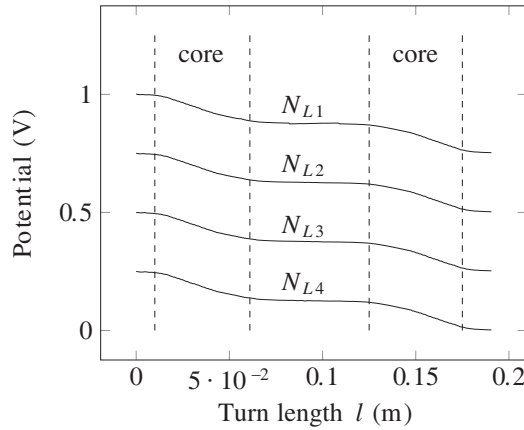


Figure 3. Simulated voltage distribution along the length of a 4-layer winding with a dielectric separation of 0.4 mm and an applied voltage of $1V_{peak}$.

2.2. Leakage Inductance

Conventionally, the leakage inductance of the planar transformer is calculated based on the magnetic field energy stored inside the dielectric volume and the conductor volume. However, it has been shown in [25] that the leakage magnetic energy within the conductors decreases with frequency due to skin effect and becomes negligible at high frequency. The leakage energy within the conductor further becomes negligible when an infinitesimally thin conductor is assumed. For simplicity sake, a frequency-independent model of leakage inductance is used in the planar transformer model. Magnetic leakage energy storage within the conductors is thus ignored. Furthermore, it can be argued that these simplifications result in the minimal value for leakage inductance, which is expected to present an upper-bound for the theoretical bandwidth.

The leakage inductance of planar transformers can be calculated based on the energy storage of the H -field in the winding volume. As the H -field only varies in the vertical direction, the integral can be written as a function of vertical displacement x as follows.

$$L_k = \frac{\mu_0 l_t b_w}{I_p^2} \int H^2 dx \quad (3)$$

The H -field generated per layer can be given as Eq. (4).

$$H = \frac{nI_{P/S}}{b_w} \quad (4)$$

The leakage magnetic field pattern of a 2:6 transformer is found using FEKO simulation and plotted in Fig. 4. It may be noted that the conductors are assumed to be much thinner than the dielectric thickness). The integral of the H field can be written as Eq. (5a), based on the resulting H -field pattern. Using Eq. (3) the leakage inductance is then found as Eq. (5b).

$$\int H^2 dx = t \left(\frac{nI_p}{b_w} \right)^2 \left[\sum_{y=1}^{N_P-1} y^2 + N_P^2 + \left(\frac{N_P}{N_S} \right)^2 \left(\sum_{z=1}^{N_S-1} z^2 \right) \right] \quad (5a)$$

$$L_k = \frac{\mu_0 t l_t n^2}{b_w} \left[\sum_{y=1}^{N_P-1} y^2 + N_P^2 + \left(\frac{N_P}{N_S} \right)^2 \left(\sum_{z=1}^{N_S-1} z^2 \right) \right] \quad (5b)$$

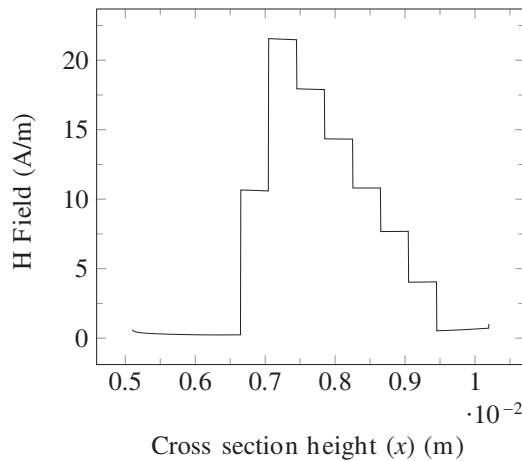


Figure 4. Simulated H -field cross section within core window of a 2:6 planar transformer with dielectric thickness of 0.4 mm. Excited by $I_P = 0.19$ A at $1V_{peak}$. Conductor thickness simulated to be negligibly small.

2.3. The Equivalent Electrical Circuit Model

The circuit model shown in Fig. 5 is proposed, as other circuit models found in literature [8, 12, 14, 26–28] use a magnetizing inductance approach that is unable to model the resonance mechanism between the secondary winding inductance and secondary self-capacitance, which is critical to analytically determine their impact on bandwidth. The non-ideal coupling behavior is captured by the inclusion of a leakage inductance element. Furthermore, the placement of the leakage inductance is disputed in literature; through trial and error, it was found that the placement of the leakage inductor in the position illustrated in Fig. 5 best matches the simulation results, and is thus found to be a more accurate description of the transformer model.

The circuit was simulated in NgSpice, and three-dimensional electromagnetic simulations were conducted in FEKO to validate the proposed electrical circuit model. The dimensions of an E64/PLT core [29] were used for simulation. The FEKO models were created and were set up such that the conductors were infinitesimally thin, and all losses such as core and dielectric losses are ignored; the materials used in the simulation were given ideal characteristics.

The specifications of the transformer simulated in FEKO are summarized in Table 2. The values of the parasitics and the winding inductances arising from the provided specifications are presented in Table 3. The simulation was done only within the frequency range where the bandwidth is expected,

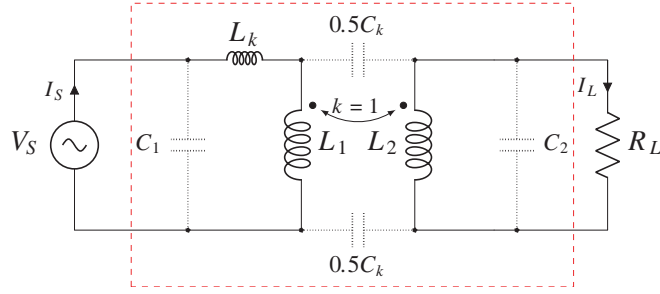


Figure 5. Proposed electrically equivalent circuit model of a planar transformer shown inside the dashed box.

Table 2. Specifications of planar transformers simulated in FEKO.

Turns Ratio	t (mm)	ϵ_r	μ_r	l_t (mm)	w (mm)
2:4	0.4	500	500	220	18.8
4:8	0.4	5	1000	220	18.8

Table 3. Values of elements in the equivalent circuit models of the planar transformer, derived using dimensions in Table 2.

Turns Ratio	C_1 (pF)	C_2 (pF)	C_k (pF)	L_1 (μ H)	L_2 (μ H)	L_k (nH)
2:4	11,527	8,645	46,110	17.55	70.20	50.36
4:8	86.45	50.43	461.10	140.40	561.63	385.12

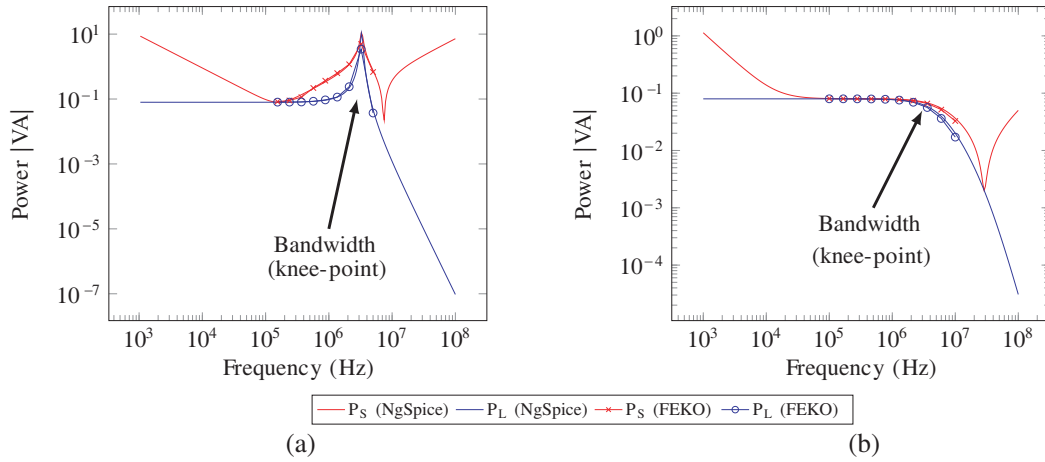


Figure 6. Comparison of power response in the frequency domain of proposed circuit model against FEKO simulation, using specifications given in Table 2 and Table 3. (a) Load and source power of a 2:4 transformer plotted in the frequency domain. A sharp knee-point is indicated on the plot. Transformer excited by 1 V sinusoidal source. (b) Load and source power of a 4:8 transformer plotted in the frequency domain. A rounded knee-point is indicated on the plot. Transformer excited by 1 V sinusoidal source.

to reduce the requirement of large computational resources. The secondary side of the circuit and the FEKO simulation model were both loaded with a load R_L of 50 ohms for demonstration purpose.

The power response of the circuit model simulated using NgSpice is then compared to FEKO simulations in Fig. 6. It may be noted that converging load and source power only represents

approximate unity power factor and not unity efficiency. Inspection of these results show that the circuit model adequately matches the planar transformer's frequency response as it is able to capture the early resonance-like knee-points accurately.

3. POWER BANDWIDTH OF THE PLANAR TRANSFORMER

The power bandwidth of the planar transformer shall be defined as the frequency beyond which the transformer's power output does not remain constant. More specifically, it is the frequency where the transformer turns ratio is not followed by the currents and voltages, resulting in the fundamental function of the transformer failing. The bandwidth of the transformer is thus the 'knee-points' indicated in Fig. 6(a) and Fig. 6(b). It can be seen that beyond the knee-points, the load voltage does not remain constant.

The electromagnetic parasitics L_k , C_k , C_1 & C_2 can be rewritten as functions of dielectric thickness t with parasitic coefficients denoted with a subscript 'c'. These expressions, Eqs. (6a)–(6d), have been derived previously in Section 2.1 and Section 2.2.

$$C_1 = \epsilon_0 \epsilon_r \frac{l_t b_w}{t} \left(\frac{N_P - 1}{N_P^2} \right) = \frac{1}{t} (C_{1c}) \quad (6a)$$

$$C_2 = \epsilon_0 \epsilon_r \frac{l_t b_w}{t} \left(\frac{N_S - 1}{N_S^2} \right) = \frac{1}{t} (C_{2c}) \quad (6b)$$

$$C_k = \epsilon_0 \epsilon_r \frac{l_t b_w}{t} = \frac{1}{t} (C_{kc}) \quad (6c)$$

$$L_k = \frac{\mu_0 t l_t n^2}{b_w} \left[\sum_{y=1}^{N_P-1} y^2 + N_P^2 + \left(\frac{N_P}{N_S} \right)^2 \left(\sum_{z=1}^{N_S-1} z^2 \right) \right] = t (L_{kc}) \quad (6d)$$

With all the relevant parasitics analytically described, the circuit model presented in Fig. 5 can be analyzed using available circuit analysis techniques. In this case, mesh analysis was used to derive expressions for the currents and voltages within the circuit model in the frequency domain. The load current was then used to derive the expression for the load power as a function of frequency. Due to the load power expression being unwieldy, an approximation of the load power denominator expression given in (A3) in Appendix A. This expression can be rewritten by substituting the parasitics as functions of dielectric thickness and parasitic coefficients, as described in Eqs. (6a), (6b), (6c) & (6d). This rewritten denominator expression given in (A4a) is used to find the frequency poles of the load power expression as given in Eq. (A4b) in Appendix A, which give the exact location of the bandwidth of the structure as a function of dielectric thickness.

4. DIELECTRIC THICKNESS OPTIMIZATION

The bandwidth of the structure has been analytically derived as a function of dielectric thickness in the previous section. The general effect of dielectric thickness on the bandwidth is shown in Fig. 7 for arbitrary values of parasitic coefficients. From inspection of these plots, the optimum dielectric thickness value can be said to be the value of the dielectric thickness that results in the highest bandwidth. Thus, the choice of optimum thickness results in maximum bandwidth for a given set of parasitic coefficients. The optimum thickness is derived in Appendix B.

Inspection of Fig. 7 shows that there seems to be a sharp transition where the bandwidth no longer appears to be a function of dielectric thickness. However, the transition is magnified in effect due to the use of the log-scale for the plot. Furthermore, a deeper analysis of the expression (A4a) in Appendix B reveals that the bandwidth function is made up of terms that are products of dielectric thickness together with terms that contain just the parasitic coefficients described in Section 3 (these terms do not contain the thickness variable, thus remain constant in magnitude). Below some optimum thickness value (t_{opt} , in Fig. 7), the terms that are products of dielectric thickness get too small compared to the magnitude of the terms containing the parasitic coefficients, resulting in negligible overall effect on the bandwidth.

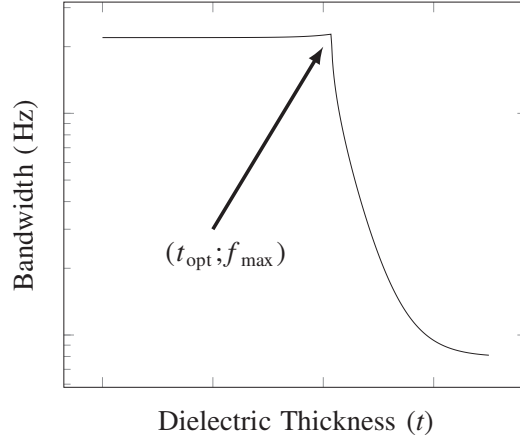


Figure 7. Example plot showing the effect of dielectric thickness on the theoretical bandwidth. Arbitrary parasitic coefficient parameters used for illustration.

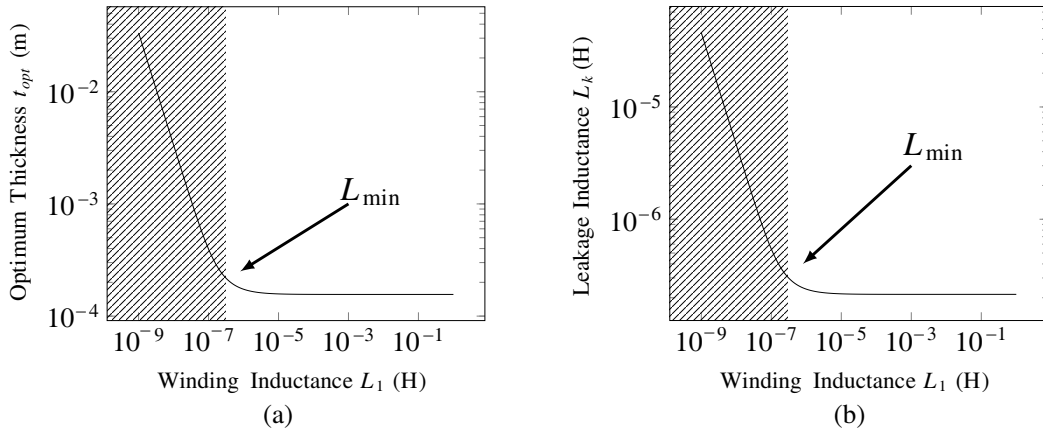


Figure 8. Plots showing the influence of winding inductance on optimum thickness resulting leakage inductance values with arbitrary parameters. The shaded region represents values that are not feasible, as the winding inductance can never be less than the leakage inductance in reality. (a) Influence of primary winding inductance on optimum dielectric thickness. (b) Influence of primary winding inductance on the resulting leakage inductance.

It may be noted that the winding inductance also appears to have some influence on the optimum dielectric thickness and the maximum bandwidth. This influence can be seen from inspection of the plots presented in Fig. 8, where the optimum dielectric thickness value, the resultant leakage inductance L_k and the maximum bandwidth are thus plotted as a function of primary winding inductance L_1 in Fig. 8. It should be noted that the leakage inductance plot in Fig. 8(b) is calculated using the optimum dielectric thickness values presented in Fig. 8(a).

It can be seen from this plot that the primary winding inductance stops having an influence on the optimum dielectric thickness and bandwidth beyond a certain winding inductance value. This value is given as L_{\min} in Eq. (7) (derivation shown in Appendix B). Far beyond L_{\min} , the optimum dielectric thickness and the maximum bandwidth converge to their asymptote values t'_{opt} & f'_{max} , given in Eq. (8a) and Eq. (8b).

$$L_{\min} = \frac{3}{2a_r^2} R_L \sqrt{L_{k_c} (-4C_{2_c} a_r^2 - C_{k_c} (a_r^2 - 2a_r + 1))} \quad (7)$$

$$t'_{opt} = \lim_{L_1 \rightarrow \infty} t_{opt} = \frac{R_L}{a_r^2} \sqrt{\frac{(4C_{2_c} + C_{k_c}) a_r^2 - 2C_{k_c} a_r + C_{k_c}}{L_{k_c}}} \quad (8a)$$

$$f'_{\max} = \lim_{L_1 \rightarrow \infty} f_{\max} = \left| \frac{2jL_{k_c}a_r^2t'_{opt} + 2\sqrt{(L_{k_c}a_r^4t'^2_{opt} + ((4C_{2_c} + C_{k_c})a_r^2 - C_{k_c}(2a_r - 1))R_L^2)L_{k_c}}}{((4C_{2_c} + C_{k_c})L_{k_c}a_r^2 - 2C_{k_c}L_{k_c}a_r + C_{k_c}L_{k_c})R_L} \right| \quad (8b)$$

Given that the core is designed such that the winding inductance is much greater than L_{\min} , the t'_{opt} expression can be used to conveniently choose the optimum dielectric thickness. This ensures that the resulting bandwidth will be the largest possible for a given planar transformer configuration.

It should also be noted that the primary winding inductance L_1 must be greater than or equal to L_{\min} , as a winding inductance below this value gives an optimum thickness that results in a leakage inductance value that is theoretically greater than the winding inductance. Although this is possible in a circuit model from which these expressions have been derived, it is physically unrealizable. This physically non-realizable region is shaded as shown in Fig. 8. Maximum theoretical bandwidth cannot be guaranteed by forcing the resultant dielectric optimum thickness value, as the mathematical circuit model then starts to depart from reality.

It could be argued based on Fig. 7 that the smallest available dielectric thickness could be used in most cases. However, this is not a good design procedure as the lower limit for the dielectric thickness is essentially based on the dielectric breakdown. Furthermore, without knowing the optimum thickness value, there is no way to know that the transformer is designed for maximum bandwidth. It may also be that the optimum dielectric thickness is not sufficient to prevent dielectric breakdown in certain cases, when a large voltage is applied across the windings. One way to overcome this is to redesign the transformer parameters in (8a) such that the resulting optimum thickness is above the threshold for dielectric breakdown. Of course, another option is to choose a more resilient dielectric material.

5. DESIGN EXAMPLE

A 4:1 low power, high frequency transformer is designed as an example to show the benefits of optimizing the bandwidth and dielectric thickness. The specifications of the transformer are given in Table 4.

Table 4. Requirements of transformer design.

PARAMETER	VALUE
Frequency	1 MHz
Power	50 W
Turns Ratio	4:1
n	1
V_{in}	100 V
V_{out}	25 V
B_{peak}	0.2 T

5.1. Core & Winding Dimension Design

The minimum cross sectional area for the magnetic flux to avoid flux saturation is given as Eq. (9).

$$A_{\phi} \geq \frac{V_{in}}{4fN_P B_{peak}} \quad (9)$$

The dielectric layer must then accommodate for this area by selection of either l_c or l_w (illustrated in Fig. 1) such that the product is equal to A_{ϕ} as given by Eq. (9); l_c or l_w should be less than $\sqrt{A_{\phi}}$ to maintain planar form.

The width of the core window b_w can then be chosen, after which the dimensions of the dielectric layer D_l & D_w can be calculated as given in Eqs. (10a) & (10b).

$$D_l = l_c + 2b_w \quad (10a)$$

$$D_w = l_w + 2b_w \quad (10b)$$

The primary winding inductance is thus calculated using Eq. (11).

$$L_1 = \begin{cases} \left[\frac{\mu_0 \mu_r}{l_m} n^2 A_\phi \left(N_P + 2 \binom{N_P}{2} \right) \right] & \text{if } N_P > 1 \\ \left[\frac{\mu_0 \mu_r}{l_m} n^2 A_\phi \right] & \text{if } N_P = 1 \end{cases} \quad (11)$$

5.2. Optimum Thickness and Discussion

The specifications have led to the optimized transformer design with parameters specified in Table 5 (the blanks represent values that are unchanged). The values in the table were calculated based on expressions shown in Section 5.1, Section 4 and Section 2. The power transfer characteristics in the frequency domain for the optimized transformer are presented in Fig. 9(a). The effect of dielectric thickness on the bandwidth is presented in Fig. 9(b) for the designed winding inductance value. A dielectric thickness of 0.4 mm is chosen as an example of a standard thickness.

Table 5. Transformer design parameters.

PARAMETER	VALUE (optimized)	VALUE (non-optimized)
μ_r/ϵ_r	–	1000/5
L_{\min}	–	2.71 μH
L_1	51.5 μH	44.4 μH
R_L	–	12 Ω
t	0.156 mm	0.4 mm
f_{\max}	286 MHz	58.5 MHz
b_w	–	1 mm
l_w	–	2.23 mm
l_c	–	14 mm
l_m	12.20 mm	14.14 mm
L_k	214 nH	549 nH
C_1	2 pF	0.75 pF
C_k	10.3 pF	4 pF
C_2	–	≈ 0

It can be seen in the design example from Fig. 9(b) & Table 5 that the bandwidth is optimized when an optimum dielectric thickness of 0.156 mm is used. An approximate 389% improvement in bandwidth is found compared to when a standard thickness of 0.4 mm is used. It should be observed from Fig. 9(b) that the bandwidth is sensitive to the change in dielectric thickness value above a certain optimum threshold, which is t_{opt} . However, it can also be seen that the optimum thickness in this case is merely the maximum thickness that should be used, as using a thickness less than the optimum thickness does not significantly affect the bandwidth.

It may be noted that the lower limit for the choice of dielectric thickness depends on the breakdown of the dielectric material. In cases where the optimum thickness is lower than the thickness needed to prevent the dielectric breakdown of the material, a better dielectric material may be used, if the primary goal is to maintain high bandwidth.

It can be seen from Table 5 that the designed primary winding inductance is greater than L_{\min} . This indicates that the optimization of the dielectric thickness ensures the highest possible bandwidth for the given parameters such as the turns ratio, load resistance, track width and track length. Of course the winding inductance can be constructed to be lower than L_{\min} given the same parameters. However, if this is the case, maximized bandwidth cannot be guaranteed even if the optimum dielectric thickness is chosen.

Inspection of the frequency characteristics of the structure shown in Fig. 9(a) shows that the practical operational bandwidth of the transformer starts at 1 MHz and ends at 285 MHz. The lower

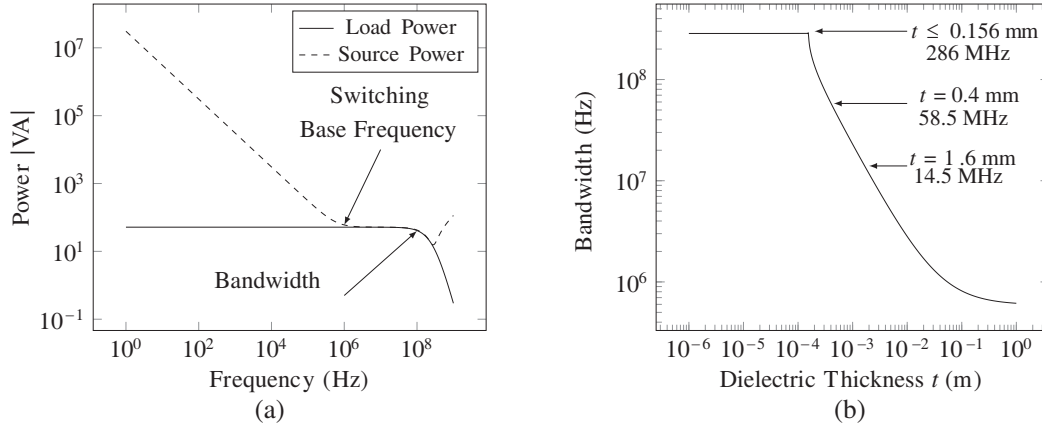


Figure 9. Plots showing characteristics of designed transformer. (a) Optimised power transfer characteristics of source and load power in the frequency domain. The difference in the magnitude of the load and source power is due to changing power-factor as a function of frequency. (b) Influence of dielectric thickness on the bandwidth. It can be observed that the bandwidth is very sensitive to the dielectric thickness above an optimum thickness value of 0.156 mm.

end of the frequency bandwidth is loosely based on the choice of switching frequency chosen in the initial design process. The improvement of bandwidth would allow for more harmonics of the switching waveform to be passed through the transformer undistorted.

Furthermore, from Table 5 it is found that the self capacitance of the secondary winding is considered zero. It is in fact a non-zero value, given that there exist some capacitance between the terminals of each winding layer. However, this capacitance is relatively much smaller than the coupling capacitance C_k and can thus be considered negligible.

6. IMMEDIATE DIRECT APPLICATION

This work has presented a minimum primary winding inductance L_{min} to guarantee maximum theoretical bandwidth for a chosen optimum thickness t_{opt} . Air-core transformers are very similar to planar transformers; their structures are similar with the only difference being the lack of a ferrite core. Hence, it can be argued that air-core transformers [30, 31] will benefit most from this optimization process as there is now a lower limit for the winding inductance. Furthermore, air-core transformers tend to have a higher bandwidth (possibly approaching theoretical bandwidth) due to the absence of non-linear ferrite losses that could potentially limit the bandwidth.

7. CONCLUSION

The bandwidth of the transformer (as was defined in Section 3) has been described analytically as functions of the intrinsic electromagnetic parasitics (stray capacitance and leakage inductance), which are functions of dielectric thickness. The optimum dielectric thickness was then analytically derived by analyzing its influence on the bandwidth of the transformer.

This paper has shown that the dielectric thickness of a planar transformer windings can be optimized such that the theoretical bandwidth limit of the transformer is maximized. It has also shown that the bandwidth is very sensitive to the dielectric thickness beyond a certain threshold t_{opt} .

It has been shown using a design example that optimization of dielectric thickness results in a theoretical bandwidth improvement of approximately 389% compared to the use of a standard dielectric thickness of 0.4 mm.

It can be argued that planar transformers with various different physical winding arrangements can be described using the equivalent circuit model presented in this paper, though the calculations of the elements within the model might slightly vary. However the principles of evaluating the elements remain

the same. Furthermore, it should also be noted that the solutions for the optimum dielectric thickness and maximum bandwidth are only unique to the circuit model from which they are derived. Similar solutions can be derived from other circuit models, and are expected to be numerically approximate to the ones in this paper. This is true as long as the same bandwidth definition discussed in this paper is used, and the frequency characteristics of the alternate circuit models are accurate.

It is expected that practical bandwidth should at best approach the theoretical bandwidth, due to the known non-ideal nature of reality. These results can thus aid in planar transformer design by circumventing the requirements of large computational resources for iterative three-dimensional FEM simulations. Furthermore, it is argued that these results are directly applicable to aid the design process air-core transformers for high bandwidth applications.

ACKNOWLEDGMENT

Thanks are extended to Dr. R. Dreyer, for the generous use of the Crunchyard service for FEKO simulations. The authors also acknowledge the funding from the National Research Foundation and the University of the Witwatersrand, South Africa, in support of this research.

APPENDIX A. MESH CIRCUIT AND BANDWIDTH DERIVATION

The circuit from which the relevant expressions are derived is given in Fig. A1. The sources V_{m1} and V_{m2} are mutual voltages induced by winding inductances L_2 and L_1 respectively. V_s is assumed to be 1 V. All following expressions are derived from analysis of the mesh equations of the equivalent circuit, shown in Eq. (A1).

$$M = k\sqrt{L_1L_2}, \quad k = 1 \quad (\text{A1a})$$

$$V_{m1} = j\omega M(I_3 - I_4) \quad (\text{A1b})$$

$$V_{m2} = j\omega M(I_2 - I_3) \quad (\text{A1c})$$

$$V_S = \frac{I_1 - I_2}{j\omega C_1} \quad (\text{A1d})$$

$$0 = \frac{I_2 - I_1}{j\omega C_1} + I_2 L_k + V_{m1} + (I_2 - I_1)L_2 \quad (\text{A1e})$$

$$0 = (I_3 - I_2)L_1 + (I_3 - I_4)L_2 + 2\frac{I_3}{0.5j\omega C_k} - V_{m1} + V_{m2} \quad (\text{A1f})$$

$$0 = (I_4 - I_3)L_2 - V_{m2} + \frac{(I_4 - I_5)}{j\omega C_2} \quad (\text{A1g})$$

$$0 = \frac{(I_5 - I_4)}{j\omega C_2} + I_5 R_L \quad (\text{A1h})$$

The load power expression of the transformer circuit model is given in Eq. (A2c). The poles of the load power expression can be found by solving for ω of Eq. (A2b); the roots of the 4th order expression

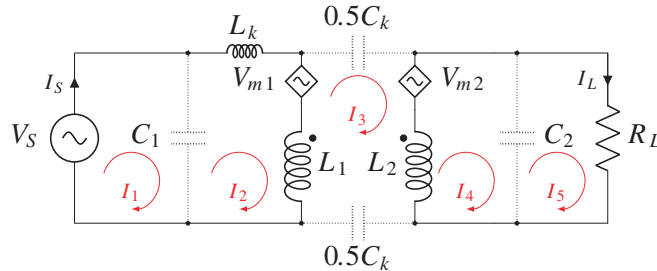


Figure A1. Transformer equivalent circuit model showing mesh current loops.

are unwieldy to find. An approximation of the denominator expression is thus used; this expression is given in Eq. (A3). It may be noted that all expressions are taken as absolute values as the load power dissipated is referred to the secondary side of the transformer.

$$\left| P_{L(num)}(\omega) \right| = \left| R_L C_k^2 (L_1 L_2 - M^2) \omega^4 - 8 R_L C_k M (L_1 L_2 - M^2) \omega^2 + 16 M^2 R_L \right| \quad (A2a)$$

$$\left| P_{L(den)}(\omega) \right| = \left| \left(C_2 C_k L_k R_L (L_1 L_2 - M^2) \omega^4 + j C_k L_k (L_1 L_2 - M^2) \omega^3 - (C_k L_k (L_1 - 2M) - (4C_2 + C_k) M^2 + (4C_2 + C_k))(L_1 + L_k) \omega^2 + j 4(L_1 L_2 + L_2 L_k - M^2) \omega + 4 R_L (L_1 + L_k) \right)^2 \right| \quad (A2b)$$

$$|P_L(\omega)| = \left| \frac{P_{L(num)}(\omega)}{P_{L(den)}(\omega)} \right| \quad (A2c)$$

$$\left| P'_{L(den)}(\omega) \right| = \left| - \left((C_k L_k (L_1 - 2M) - (4C_2 + C_k) M^2 + (4C_2 + C_k))(L_1 + L_k) \omega^2 + j 4(L_1 L_2 + L_2 L_k - M^2) \omega + 4 R_L (L_1 + L_k) \right)^2 \right| \quad (A3)$$

The coefficients of ω in Eq. (A3) can be rewritten as functions of dielectric thickness t by defining the parasitics L_k , C_1 , C_2 & C_k as functions of t ; the polynomial is then equated to zero to solve for roots of ω as given in Eq. (A4a). The coefficients are given in Eqs. (A5a)–(A5c). The general 3 dB bandwidth of the transformer is thus given as the root of the expression in Eq. (A4a) as Eq. (A4b).

$$0 = a\omega^2 + b\omega + c \quad (A4a)$$

$$\text{Bandwidth (rad/s)} = \left| \frac{-b + \sqrt{b^2 - 4ac}}{2a} \right| \quad (A4b)$$

$$a = - (C_{k_c} L_{k_c} t (L_1 - 2M) - (4C_{2_c} + C_{k_c})(M^2 - L_2(L_{k_c} t + L_1))) R_L \quad (A5a)$$

$$b = j 4t((L_{k_c} t + L_1)L_2 - M^2) \quad (A5b)$$

$$c = 4t(L_{k_c} t + L_1)R_L \quad (A5c)$$

APPENDIX B. OPTIMUM DIELECTRIC THICKNESS DERIVATION

The optimum dielectric thickness is derived by considering the discriminant of the bandwidth expression given in Eq. (A4b) in Appendix A. The expression is written as function of thickness t as given in Eq. (B1); the coefficients for the expression are given in Eqs. (B3a)–(B3c). The optimum thickness is then the root of Eq. (B1) and is given in Eq. (B4). The maximum bandwidth f_{max} is found as Eq. (B5) with t equal to t_{opt} .

$$0 = b^2 - 4ac = a_x t^2 + b_x t + c_x \quad (B1)$$

At this point, a few important substitutions are made in Eq. (B2), where a_r is the turns ratio of the transformer.

$$L_2 = a_r^2 L_1 \quad (B2a)$$

$$M = \sqrt{L_1 L_2} = a_r L_1 \quad (B2b)$$

$$a_x = -16 L_1^2 L_{k_c}^2 a_r^4 \quad (B3a)$$

$$b_x = 16(L_{k_c}^2 (a_r^2 (4C_{2_c} + C_{k_c}) - C_{k_c} (2a_r - 1))) L_1 R_L^2 \quad (B3b)$$

$$c_x = 16(L_{k_c} (a_r^2 (4C_{2_c} + C_{k_c}) - C_{k_c} (2a_r - 1))) L_1^2 R_L^2 \quad (B3c)$$

$$t_{opt} = \left| \frac{-b_x - \sqrt{b_x^2 - 4a_x c_x}}{2a_x} \right| \quad (B4)$$

$$f_{max} = \left. \frac{-b + \sqrt{b^2 - 4ac}}{2a} \right|_{t=t_{opt}} \quad (B5)$$

The value of L_{min} is found by solving for the knee-point of the plot shown in Fig. 8(a). This point can be found by analyzing t_{opt} as a function of winding inductance L_1 , and solving for the root of L_1 . It is found that the root of L_1 lies in the discriminant of Eq. (B4) given in Eq. (B6), derived from Eq. (B4). L_{min} is then found by solving for L_1 root in Eq. (B6).

$$0 = b_x^2 - 4a_x c_x \quad (B6)$$

REFERENCES

1. Estrov, A., "Power transformer design for 1 MHz resonant converter," *High Frequency Power Conv. Conf. Rec.*, 36–54, 1986.
2. Estrov, A., "Low-profile planar transformer for use in off-line switching power supplies," U.S. Classification 336/198, 336/183, 336/200, 336/232; International Classification H01F27/32, H01F19/04, H01F5/02, H01F27/28; Cooperative Classification H01F27/2804, H01F41/043, H01F19/04, H01F5/02; European Classification H01F19/04, H01F5/02, Apr. 1991.
3. Oshiro, O., H. Tsujimoto, and K. Shirae, "Structures and characteristics of planar transformers," *IEEE Translation Journal on Magnetism in Japan*, Vol. 4, No. 5, 332–338, May 1989.
4. Van Der Linde, D., C. A. M. Boon, and J. B. Klaassens, "Design of a high-frequency planar power transformer in multilayer technology," *IEEE Transactions on Industrial Electronics*, Vol. 38, No. 2, 135–141, Apr. 1991.
5. Djuric, S., G. Stojanovic, M. Damjanovic, and E. Laboure, "Analysis of the coupling effect in different meander-type winding planar transformers," *IEEE Transactions on Magnetism*, Vol. 49, No. 7, 3993–3996, Jul. 2013.
6. Djuric, S. M. and G. M. Stojanovic, "A compact planar transformer with an improved winding configuration," *IEEE Transactions on Magnetism*, Vol. 50, No. 11, 1–4, Nov. 2014.
7. Ouyang, Z. and M. A. E. Andersen, "Overview of planar magnetic technology — Fundamental properties," *IEEE Transactions on Power Electronics*, Vol. 29, No. 9, 4888–4900, Sep. 2014.
8. Ouyang, Z., O. C. Thomsen, and M. A. E. Andersen, "Optimal design and tradeoff analysis of planar transformer in high-power DC-DC converters," *IEEE Transactions on Industrial Electronics*, Vol. 59, No. 7, 2800–2810, Jul. 2012.
9. Lu, J. W., F. P. Dawson, and S. Yamada, "Analysis of high frequency planar sandwich transformers for switching converters," *IEEE Transactions on Magnetism*, Vol. 31, No. 6, 4235–4237, Nov. 1995.
10. Tria, L. A. R., D. Zhang, and J. E. Fletcher, "Planar PCB transformer model for circuit simulation," *IEEE Transactions on Magnetism*, Vol. 52, No. 7, 1–4, Jul. 2016.
11. Margueron, X., A. Besri, Y. Lembeye, and J. P. Keradec, "Current sharing between parallel turns of a planar transformer: Prediction and improvement using a circuit simulation software," *IEEE Transactions on Industry Applications*, Vol. 46, No. 3, 1064–1071, May 2010.
12. Buccella, C., C. Cecati, and M. Di Domenico, "An accurate equivalent circuit of high power/high frequency planar transformers using FEM," *International Symposium on Power Electronics, Electrical Drives, Automation and Motion, 2008. SPEEDAM 2008*, 1300–1305, Jun. 2008.
13. Chen, W., Y. Yan, Y. Hu, and Q. Lu, "Model and design of PCB parallel winding for planar transformer," *IEEE Transactions on Magnetism*, Vol. 39, No. 5, 3202–3204, Sep. 2003.
14. Cove, S. R., M. Ordonez, F. Luchino, and J. E. Quaicoe, "Applying response surface methodology to small planar transformer winding design," *IEEE Transactions on Industrial Electronics*, Vol. 60, No. 2, 483–493, Feb. 2013.

15. De Jong, E. C. W., B. J. A. Ferreira, and P. Bauer, "Toward the next level of PCB usage in power electronic converters," *IEEE Transactions on Power Electronics*, Vol. 23, No. 6, 3151–3163, Nov. 2008.
16. Zhang, K., T. X. Wu, N. Kutkut, J. Shen, D. Woodburn, L. Chow, W. Wu, H. Mustain, and I. Batarseh, "Modeling and design optimization of planar power transformer for aerospace application," *Proceedings of the IEEE 2009 National Aerospace Electronics Conference (NAECON)*, 116–120, Jul. 2009.
17. Bowen, D., A. Lee, C. Krafft, and I. D. Mayergoyz, "Performance effects of device scale and core aspect-ratio on dielectric-core circuit board transformers," *Journal of Applied Physics*, Vol. 115, No. 17, 17E717, 2014.
18. Panchal, C. and J. W. Lu, "High frequency planar transformer (HFPT) for universal contactless battery charging platform," *IEEE Transactions on Magnetics*, Vol. 47, No. 10, 2764–2767, Oct. 2011.
19. Saravi, S. E., A. Tahani, F. Zare, and R. A. Kordkheili, "The effect of different winding techniques on the stray capacitances of high frequency transformers used in yback converters," *IEEE 2nd International Power and Energy Conference, 2008. PECon 2008*, 1475–1478, Dec. 2008.
20. Maswood, A. I. and L. K. Song, "Design aspects of planar and conventional SMPS transformer: A cost benefit analysis," *IEEE Transactions on Industrial Electronics*, Vol. 50, No. 3, 571–577, Jun. 2003.
21. Ambatipudi, R., H. B. Kotte, and K. Bertilsson, "High performance planar power transformer with high power density in MHz frequency region for next generation switch mode power supplies," *2013 Twenty-Eighth Annual IEEE Applied Power Electronics Conference and Exposition (APEC)*, 2139–2143, Mar. 2013.
22. Bowen, D., A. Lee, C. Krafft, and I. D. Mayergoyz, "Design control of performance in nested and interleaved winding printed circuit board transformers for ethernet applications," *IEEE Transactions on Magnetics*, Vol. 49, No. 7, 4013–4016, Jul. 2013.
23. Bowen, D., A. Lee, C. Krafft, and I. D. Mayergoyz, "Zero-footprint ethernet transformers using circuit-board embedded ferrites," *Journal of Applied Physics*, Vol. 115, No. 17, 17E716, 2014.
24. Costa, E. M. M., "Planar transformers excited by square waves," *Progress In Electromagnetics Research*, Vol. 100, 55–68, 2010.
25. Ouyang, Z., J. Zhang, and W. G. Hurley, "Calculation of leakage inductance for high-frequency transformers," *IEEE Transactions on Power Electronics*, Vol. 30, No. 10, 5769–5775, Oct. 2015.
26. Li, J., Y. Shi, Z. Niu, and D. Zhou, "Modeling, simulation and optimization design of PCB planar transformer," *2005 International Conference on Electrical Machines and Systems*, Vol. 3, 1736–1739, Sep. 2005.
27. Ammouri, A., T. B. Salah, and F. Kourda, "Modeling and simulation of a high-frequency planar power transformers," *2015 4th International Conference on Electrical Engineering (ICEE)*, 1–6, Dec. 2015.
28. Tria, L. A. R., D. Zhang, and J. E. Fletcher, "High-frequency planar transformer parameter estimation," *IEEE Transactions on Magnetics*, Vol. 51, No. 11, 1–4, Nov. 2015.
29. Ferroxcube, Ferroxcube E64/PLT, <http://www.ferroxcube.com/FerroxcubeCorporateReception/datasheet/e641050.pdf>, Accessed: Mar. 28, 2017.
30. Bowen, D., I. Mayergoyz, C. Krafft, D. Kroop, and M. Beyaz, "On design of air-core ethernet transformers," *Journal of Applied Physics*, Vol. 105, No. 7, 07A307, 2009.
31. Hui, S. Y., H. S.-H. Chung, and S. C. Tang, "Coreless printed circuit board (PCB) transformers for power mosfet/igbt gate drive circuits," *IEEE Transactions on Power Electronics*, Vol. 14, No. 3, 422–430, May 1999.